

Bifurcations and global stability of synchronized stationary states in the Kuramoto model for oscillator populations

J. A. Acebrón,^{1,2,*} A. Perales,³ and R. Spigler²

¹Department of Physics, University of California, San Diego, La Jolla, California 92093

²Dipartimento di Matematica, Università di "Roma Tre," Largo San Leonardo Murialdo, 1. 00146 Roma, Italy

³Departamento de Automática, Escuela Politécnica Superior, Universidad de Alcalá, 28871 Alcalá de Henares, Spain

(Received 23 February 2001; published 25 June 2001)

Bistability between synchronized stationary states is shown to occur in large populations of nonlinearly coupled random oscillators (Kuramoto model), governed by trimodal natural frequency distributions. Numerical simulations and a numerical investigation of bifurcating states provide evidence of global stability of such states, subject to unimodal, bimodal, and trimodal frequency distributions. All this may be important in the framework of large superconducting Josephson junctions arrays, as well as of neural networks.

DOI: 10.1103/PhysRevE.64.016218

PACS number(s): 05.45.Xt, 05.20.-y, 05.40.-a, 64.60.Ht

Synchronization phenomena in large populations of nonlinearly coupled oscillators and transition from incoherence to synchronized states are rather ubiquitous in such diverse fields as biology and medicine, physics, and neural networks (cf., e.g., [1] and references therein). One of the most recent areas that may benefit from research in this subject is that of superconducting Josephson junction arrays; see [2–4].

In this paper, we investigate the existence of a *bistable* behavior between (partially) synchronized *stationary* states, occurring in large populations of nonlinearly coupled random oscillators, characterized by trimodal distributions of their natural frequencies. This has been done in the framework of the so-called Kuramoto model. It seems that, in principle, any kind of multistability might be of interest in the field of neural networks [5], since this suggests the existence of stable patterns of synchronization. In particular, there is the case of vision segmentation in neurophysiology, where in a complex image, several objects of different shape and/or color may be distinguished from each other. Multistable patterns might be instrumental in realizing such a task, under the assumption that there exist several populations of neurons, each sensitive to different features of the objects, such as horizontal or vertical lines, colors, light intensity, etc. Such populations would react in a selective way, either oscillating at different frequencies or oscillating at the same frequency but with shifted phases.

In the Kuramoto model [6–8], the one-phase oscillator probability density, $\rho(\theta, t, \omega)$, obeys, in the thermodynamic limit of infinitely many oscillators, the nonlinear Fokker-Planck equation,

$$\frac{\partial \rho}{\partial t} = D \frac{\partial^2 \rho}{\partial \theta^2} - \frac{\partial}{\partial \theta} (v \rho). \quad (1)$$

Here, $v = v(\theta, \omega, t) = \omega + K r \sin(\psi - \theta)$, where K is the coupling strength, and ω is picked from a natural frequency

distribution $g(\omega)$. The complex order parameter, $re^{i\psi}$, is given, in terms of ρ and $g(\omega)$, by

$$re^{i\psi} = \int_0^{2\pi} d\theta \int_{-\infty}^{+\infty} d\omega e^{i\theta} \rho(\theta, t, \omega) g(\omega). \quad (2)$$

Suitable initial values, 2π periodicity with respect to θ , and normalization, $\int_0^{2\pi} \rho_0(\theta, \omega) d\theta = 1$, where $\rho_0(\theta, \omega) = \rho(\theta, t, \omega)|_{t=0}$, should be prescribed for the density function ρ .

In view of the application to neural networks, obviously it is desirable to be able to control the choice of the particular synchronized state to which the system will be locked. Indeed, what should be chosen is the *initial* value, $r(0)$, of the order-parameter amplitude in Eq. (2),

$$r(0) = \int_0^{2\pi} d\theta \int_{-\infty}^{+\infty} d\omega e^{i\theta} \rho_0(\theta, \omega) g(\omega) \quad (3)$$

[see the numerical simulations below, Fig. 2(a)]. This can be done by an appropriate choice of the initial distribution, $\rho_0(\theta, \omega)$. In fact, taking, e.g., $g(\omega) = \delta(\omega)$, and expanding

$$\rho_0(\theta, 0) = \frac{a_0}{2} + \sum_{n=1}^{\infty} (a_n \cos n\theta + b_n \sin n\theta) \quad (4)$$

in Fourier series, we obtain (from the normalization condition) $a_0/2 = 1/2\pi$, leaving all the other coefficients arbitrary. Inserting into Eq. (3) $r(0) = \int_0^{2\pi} \rho_0(\theta, 0) \cos \theta d\theta = a_1 \pi$, from which $a_1 = r(0)/\pi$ is obtained, the choice for the initial distribution

$$\rho_0(\theta, 0) = \frac{1}{2\pi} + \frac{r(0)}{\pi} \cos \theta \quad (5)$$

should be made whenever the value $r(0)$ is prescribed. Clearly, any other Fourier series having the coefficients a_0 and a_1 above is equally suited for the present purposes.

In this paper, we consider a trimodal frequency distribution,

$$g(\omega) = \alpha \delta(\omega) + \frac{1-\alpha}{2} [\delta(\omega - \omega_0) + \delta(\omega + \omega_0)], \quad 0 \leq \alpha \leq 1, \quad (6)$$

*Author to whom all correspondence should be addressed. Email address: acebron@physics.ucsd.edu

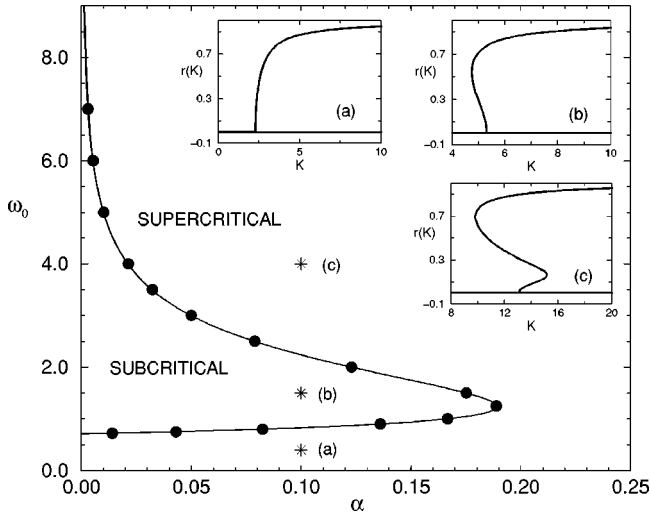


FIG. 1. Regions of subcritical and supercritical bifurcations in the space of parameters (α, ω_0) . The solid line corresponds to the analytical solution obtained from Eq. (12) setting r_3 to zero, while the points correspond to the numerical solution obtained by AUTO. The insets show the three different types of behavior for the values marked by (a), (b), and (c). D is kept fixed to 1.

where the unimodal [1] and the bimodal [7] cases are recovered when $\alpha=1$ or $\alpha=0$, respectively. When the frequency distribution is characterized by more than two peaks, certain new nontrivial features appear. In particular, we can show that the presence of a central peak (located at zero frequency) in $g(\omega)$ generates new transition regions between subcritical and supercritical bifurcations, as well as multistability among stationary solutions, for certain given values of the parameters. Bistability of synchronized states is observed and analyzed along with global stability properties with the help of AUTO [9], which is a powerful numerical code capable of computing all bifurcating solutions to a given system of ordinary differential equations. Global stability of (partially) synchronized stationary solutions, even in unimodal distributions, has been conjectured and searched for for a long time, cf. [10], and thus it seems important to provide a reasonable indication of what should be eventually proved rigorously. Indeed, here we give new evidence of a positive answer to such a question.

The stationary solution, $\rho_0(\theta, \omega)$, to problems (1) and (2) can be found as an explicit function of r , cf. [7]. Expanding it on the right-hand side of Eq. (2) in powers of r around $r=r_0$ ($r_0=0$, which corresponds to $\rho_0=1/2\pi$, the incoherent solution), Eq. (2) yields

$$r = r_0 + r_1 r + r_2 \frac{r^2}{2!} + r_3 \frac{r^3}{3!} + O(r^4), \quad (7)$$

where

$$r_n = \int_{-\infty}^{+\infty} d\omega g(\omega) \int_0^{2\pi} d\theta \cos(\psi - \theta) g_n(\theta, \omega), \quad n = 1, 2, \dots$$

and $g_n = d^n \rho_0 / dr^n|_{r=0}$ can be evaluated directly from the Fokker-Planck equation (1), being

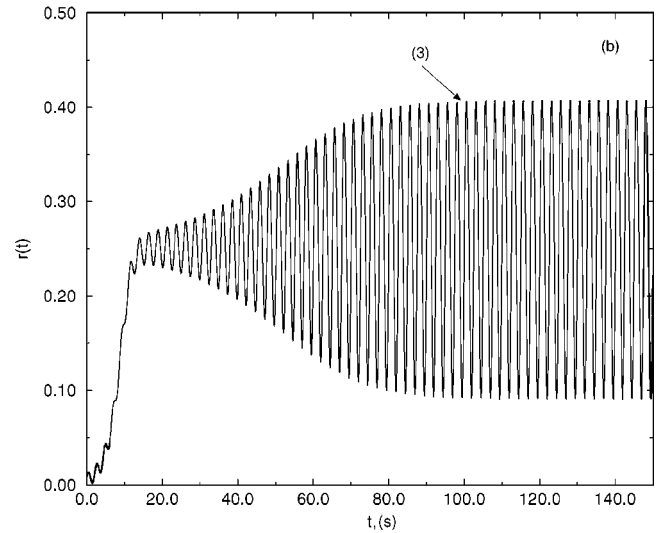
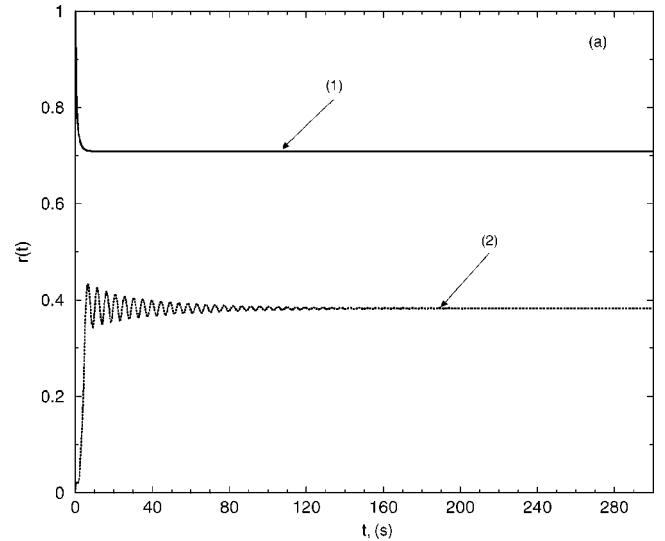


FIG. 2. Time evolution of the amplitude order parameter, $r(t)$, when $\omega_0=3.5$, $\alpha=0.3$, and $D=1$. Labels (1) to (3) identify the values of the parameters as in Figs. 4 and 6: (a) $K=8.15$; note that there are two stable stationary solutions, denoted by (1) and (2), and located in the region $K_1 < K < K_2$ in Fig. 6 corresponding to the bistability regime; (b) oscillatory solution with $K=7$, arising from the Hopf bifurcation.

$$D \frac{d^2 g_n}{d\theta^2} - \omega \frac{d g_n}{d\theta} = n K \frac{d}{d\theta} [\sin(\psi - \theta) g_{n-1}]. \quad (8)$$

Expanding in Fourier series, $g_n = \sum_{l=-\infty}^{\infty} Z_n^l(\omega) e^{i l(\theta - \psi)}$, ψ being a constant, the Fourier coefficients Z_n^l , $l=0, \pm 1, \pm 2, \dots$ satisfy, for each n , the recurrence $(i D l - \omega) Z_n^l = i n (K/2) (Z_{n-1}^{l-1} - Z_{n-1}^{l+1})$, and then

$$r_n = 2\pi \int_{-\infty}^{+\infty} d\omega g(\omega) \operatorname{Re} Z_n^1. \quad (9)$$

Observing that $Z_n^{-l} = (Z_n^l)^*$, and that $Z_0^l = 0$ when $l \neq 0$, $Z_0^0 = 1/2\pi$, and $Z_n^0 = 0$ (using the normalization condition of ρ), we get $r_2 = r_4 = 0$, and

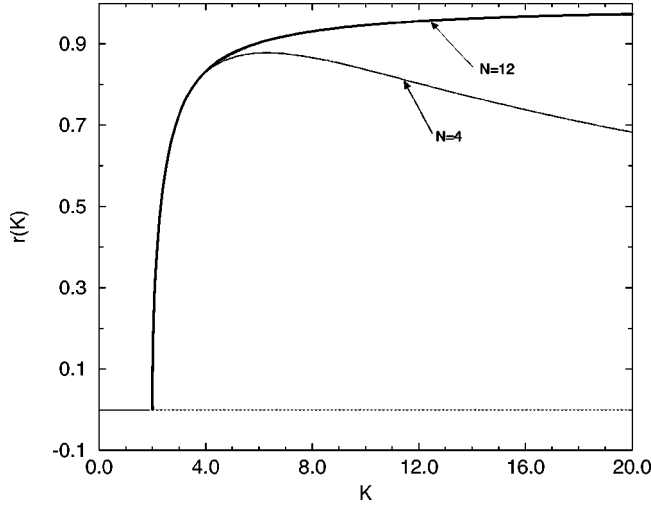


FIG. 3. Bifurcation diagram for the unimodal frequency distribution, $\alpha=1$ [i.e., $g(\omega)=\delta(\omega)$]. Two different numbers of harmonics have been chosen, $N=4,12$. The dotted line denotes the unstable solution, while the solid line corresponds to the stable solution.

$$r_1 = \frac{K}{2D} \int_{-\infty}^{+\infty} d\omega g(\omega) \frac{1}{1 + \omega^2/D^2}, \quad (10)$$

$$r_3 = \frac{3K^3}{2D^3} \int_{-\infty}^{+\infty} d\omega g(\omega) \frac{2\omega^2/D^2 - 1}{(1 + \omega^2/D^2)^2 (4 + \omega^2/D^2)}. \quad (11)$$

According to the implicit function theorem, $r=0$ is an isolated solution of Eq. (7) for $K \neq K_c$, where $K_c = 2\{\int_{-\infty}^{+\infty} [D/(D^2 + \omega^2)] g(\omega) d\omega\}^{-1}$, cf. [1].

The coefficient r_3 of r^3 in Eq. (7) may be either negative or positive, depending on the frequency distribution, $g(\omega)$. From Eq. (7), in case such a coefficient is negative, the bifurcation is *supercritical*, while, in case it is positive, it will be *subcritical*. Below, we analyze the type of bifurcation occurring correspondingly to the trimodal frequency distribution, in which case

$$r_3 = \frac{3K^3}{2D^3} \left(-\frac{\alpha}{4} + \frac{(1-\alpha)(-1+2\omega_0^2/D^2)}{(1+\omega_0^2/D^2)^2(4+\omega_0^2/D^2)} \right). \quad (12)$$

Using symbolic manipulations, we can find that, when $\alpha > \alpha_c \approx 0.189$, $r_3 < 0$ for every ω_0 , and thus the bifurcation is supercritical. On the other hand, if $\alpha < \alpha_c$, there are two frequencies, ω_c^-, ω_c^+ , such that for $\omega_0 < \omega_c^-$ or $\omega_0 > \omega_c^+$, the stationary solution branches off supercritically, while when $\omega_c^- < \omega_0 < \omega_c^+$ it branches off subcritically. In Fig. 1, a very good agreement is shown between the results of the analytical calculation of the boundary between the subcritical and the supercritical case, evaluated from Eq. (12) setting $r_3 = 0$, and the numerical solution obtained by AUTO.

Moreover, choosing conveniently the values of the parameters, *three* possible stationary solutions are found with such a frequency distribution. Only two of them, however, are

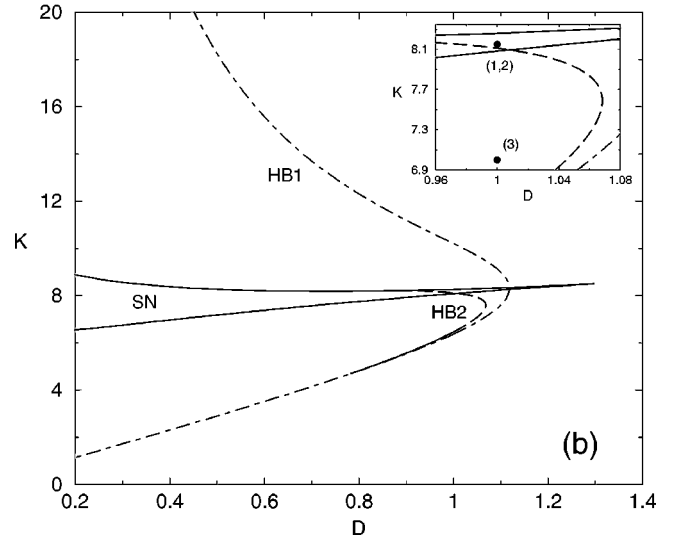
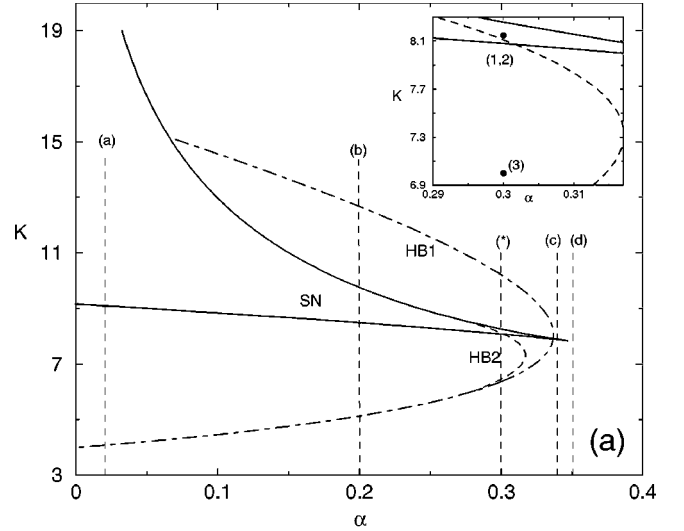


FIG. 4. Phase diagram for the trimodal frequency distribution with ω_0 kept fixed to 3.5. The solid line corresponds to a loci of saddle-node (SN) bifurcations (folds). The dotted-dashed line denotes the Hopf bifurcation (HB1) of the incoherent branch, while the dashed line corresponds to the Hopf bifurcation (HB2) of the stationary synchronized branch; (a) K versus α with $D=1$, (b) K versus D with $\alpha=0.3$. In the inset the points label the values used in the numerical simulation in Fig. 2.

stable, and this behavior can indeed be observed in the numerical simulations [see Fig. 2(a)].

The numerical study of global stability by means of AUTO has been carried out using a spectral method, which generates the hierarchy of ordinary differential equations,

$$\dot{R}_n = -n^2 D R_n + n \omega \Psi_n + n \frac{K}{2} r (R_{n-1} - R_{n+1}) - n \frac{d\psi}{dt} \Psi_n, \quad (13)$$

$$\dot{\Psi}_n = -n^2 D \Psi_n - n \omega R_n + n \frac{K}{2} r (\Psi_{n-1} - \Psi_{n+1}) + n \frac{d\psi}{dt} R_n \quad (14)$$

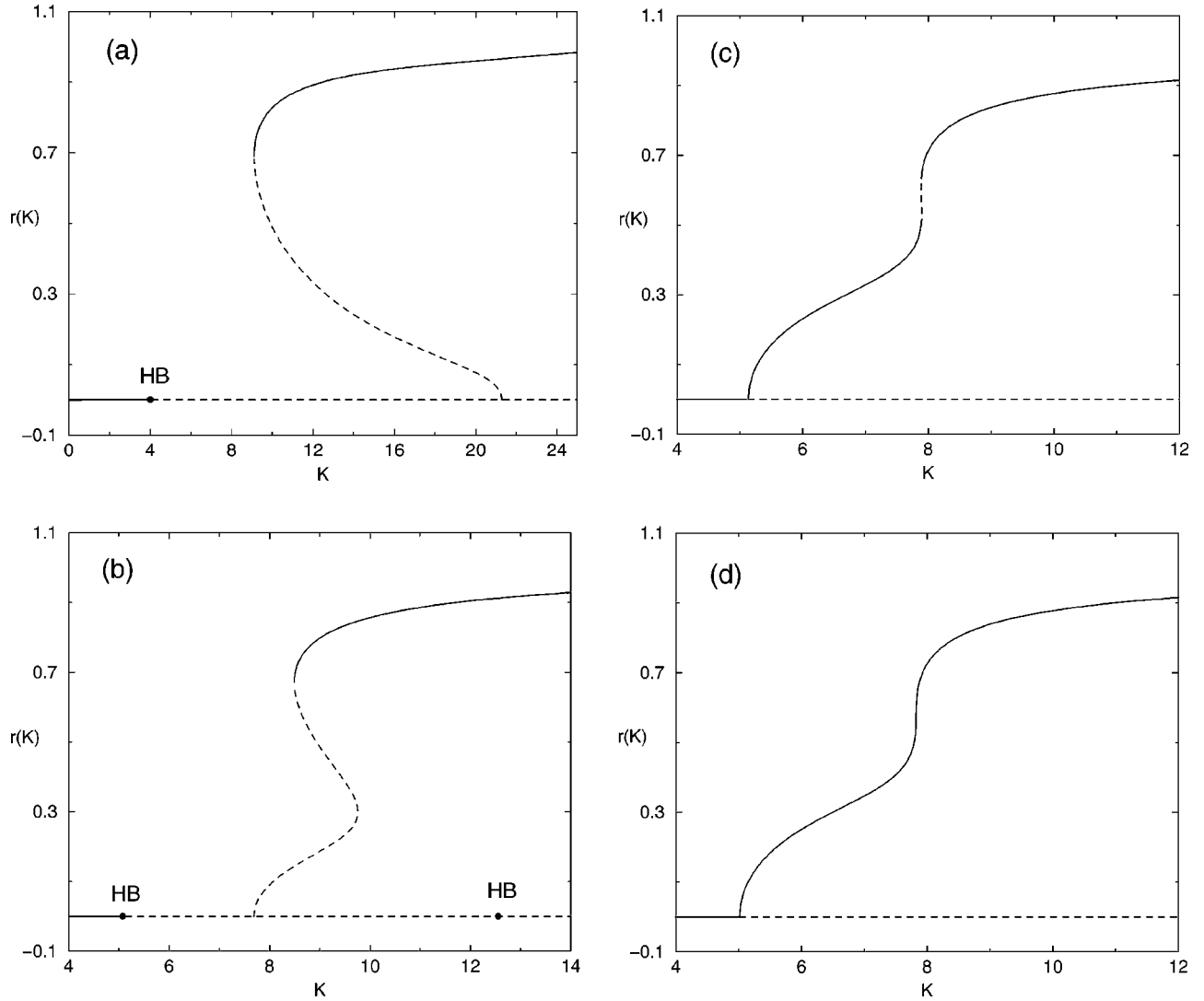


FIG. 5. Bifurcation diagram for the amplitude order parameter, r , as a function of K for several values of α ; (a) $\alpha=0.02$, (b) $\alpha=0.2$, (c) $\alpha=0.34$, and (d) $\alpha=0.35$. Parameters values are $\omega_0=3.5$ and $D=1$. The solid line corresponds to the stable solution, while the dashed line denotes the unstable one.

for the moments

$$R_n(\omega, t) = \int_0^{2\pi} \cos[n(\psi - \theta)] \rho(t, \theta, \omega) d\theta, \quad (15)$$

$$\Psi_n(\omega, t) = \int_0^{2\pi} \sin[n(\psi - \theta)] \rho(t, \theta, \omega) d\theta, \quad (16)$$

cf. [11]. The order parameter is then obtained from

$$r(t) = \int_{-\infty}^{+\infty} R_1(\omega, t) g(\omega) d\omega, \quad (17)$$

while $\int_{-\infty}^{+\infty} \Psi_1(\omega, t) g(\omega) d\omega = 0$.

In practice, we solve numerically system (14) for $n = 1, 2, \dots, N$, setting $R_{N+1} = \Psi_{N+1} = 0$. The number N of modes is chosen such that the error drops below a given tolerance, typically 10^{-12} .

In Fig. 2, the time evolution of the amplitude of the order parameter is plotted for several values of K . In Fig. 3, we

show the bifurcation diagram for the unimodal case. Note that at least $N=12$ modes are needed to reproduce the correct physical behavior, that is, the oscillators must be globally synchronized when the coupling among them is sufficiently large (in fact, $r \rightarrow 1$ as $K \rightarrow \infty$). Such a number has to be increased when K is larger or D is smaller. The phase diagram in the space of parameters (α, K) for the trimodal case is shown in Fig. 4(a). We can see the different kinds of solutions that this model yields, depending on the values of the parameters. The bifurcation diagrams, $r(K)$ versus K , for the values of α considered in Fig. 4(a), are shown in Figs. 5 and 6 [the labels (a)–(d) and (*) refer to such values as given in Fig. 4(a)]. For a given value of α , the number of stationary states equals the number of folds plus one. Note that for high values of α [case (d)], the bifurcation diagram is unfolded, supercritical, and reproduces the pattern of the unimodal case. On the other hand, for low values of α [case (a)], the bifurcation diagram presents one fold, is subcritical, and similar to the bimodal case. The other three cases [Fig. 5(b) and 5(c), and Fig. 6] exhibit two folds, i.e., three stationary

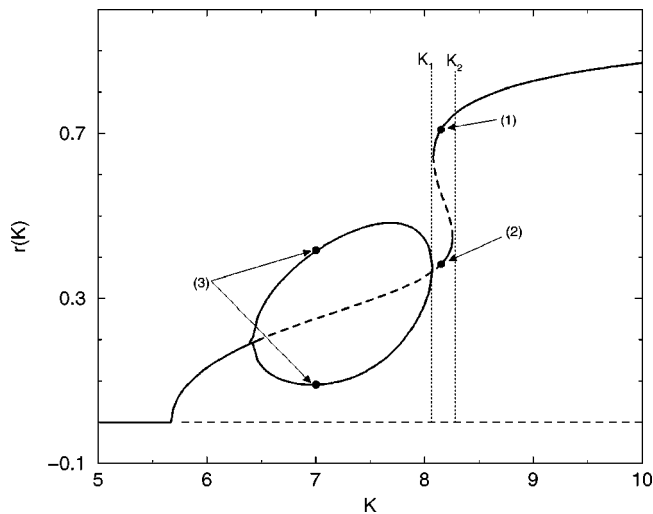


FIG. 6. Bifurcation diagram for the amplitude order parameter, r , as a function of K . The frequency distribution is trimodal, with $\omega_0=3.5$, $\alpha=0.3$, and $D=1$. The loop shows the maximum and minimum of r in the oscillatory solution. In the region $K_1 < K < K_2$, bistability between stationary synchronized solutions is observed. The points marked by (1), (2) [see Fig. 2(a)], and (3) [Fig. 2(b)] correspond to the solution obtained by direct numerical simulation of the Fokker-Planck equation. The solid line corresponds to the stable solution, while the dashed line denotes the unstable one.

states. In Fig. 4(b), we show the phase diagram in the space of parameters (D, K) , keeping α fixed. HB1 and HB2 denote the bifurcations that give rise to oscillatory behavior (Hopf bifurcations), branching off the incoherent solution or the synchronized stationary solution, respectively.

Summarizing, we conclude that a central peak in the natural frequency distribution plays an important role, in that it allows for the existence of bistability between stationary solutions. It should also be stressed that numerical evidence for *global* stability of the stationary synchronized states has been given, numerically, using AUTO. All this could be important for the dynamics of superconducting Josephson junction arrays and in neural network systems. In fact, switching between two synchronized stationary states, which may play a role in such devices, as well as in associative memories, can be realized changing the initial conditions.

The authors are indebted to C. J. Pérez Vicente, for advice concerning applications of multistability concepts to neural systems, and to L. L. Bonilla for his interest in this work. A.P. thanks J. Galán for having introduced him to the subject of numerical bifurcations. J.A.A. acknowledges support by the Office of Naval Research (Code 331). This work has been supported, in part, by UNESCO under Contract No. UVO-ROSTE 875.704.0, the Italian GNFM-CNR (now GNFM-INdAM), and Italian MURST funds. All computations were conducted at CASPUR, Rome.

-
- [1] S.H. Strogatz and R.E. Mirollo, *J. Stat. Phys.* **63**, 613 (1991).
 [2] K. Wiesenfeld, P. Colet, and S.H. Strogatz, *Phys. Rev. Lett.* **76**, 404 (1996); *Phys. Rev. E* **57**, 1563 (1998).
 [3] K. Park and M.Y. Choi, *Phys. Rev. B* **56**, 387 (1997).
 [4] T. Van Duzer and C. W. Turner, *Superconductive Devices and Circuits* (Prentice Hall, Upper Saddle River, NJ, 1999).
 [5] *Nonlinear Dynamics and Neural Networks, Proceedings of the 63rd W.E. Heraeus Seminar, Friedrichsdorf*, edited by H. G. Schuster (VCH, Weinheim, 1999).
 [6] Y. Kuramoto, *Self-entrainment of a Population of Coupled Nonlinear Oscillators*, in *International Symposium on Mathematical Problems in Theoretical Physics*, edited by H. Araki, Lecture Notes in Physics Vol. 39 (Springer, New York, 1975), pp. 420–422; *Chemical Oscillations, Waves, and Turbulence* (Springer, Berlin, 1984).
 [7] L.L. Bonilla, J.C. Neu, and R. Spigler, *J. Stat. Phys.* **67**, 313 (1992).
 [8] L.L. Bonilla, C.J. Pérez Vicente, and R. Spigler, *Physica D* **113**, 79 (1998).
 [9] E. J. Doedel, AUTO: Software for continuation and bifurcation problems in ordinary differential equations, California Institute of Technology, 1997.
 [10] S.H. Strogatz, *Physica D* **143**, 1 (2000).
 [11] J.A. Acebrón, and L.L. Bonilla, *Physica D* **114**, 296 (1998).